JOURNAL OF APPLIED ELECTROCHEMISTRY 26 (1996) 639–645

Electrochemical absorption–desorption of hydrogen on multicomponent Zr–Ti–V–Ni–Cr–Fe alloys in alkaline solution

M. KOPCZYK, G. WÓJCIK, G. MŁYNAREK, A. SIERCZYŃSKA

Centralne Laboratorium Baterii i Ogniw, PL 61-362 Poznań, Forteczna 12/14, Poland

M. BEŁTOWSKA-BRZEZINSKA*

Faculty of Chemistry, A. Mickiewicz University, PL 60-780 Poznań, Grunwaldzka 6, Poland

Received 2 May 1995; revised 6 November 1995

Multicomponent Zr–Ti–V–Ni–Cr–Fe and Zr–Ti–V–Ni–Cr alloy electrodes, with various Ti and Zr ratios, have been studied in alkaline solution by means of potentiodynamic current–overvoltage and galvanostatic overpotential–time responses during long-term continuous and intermittent charge–discharge cycles. The pressure–composition isotherms for absorption/desorption of hydrogen, evaluated from the equilibrium potential, have been compared with the gas phase isotherms. The kinetic data demonstrate the reversibility of hydrogen electrosorption in the investigated systems. An increased discharge efficiency has been established for electrodes with lower values of both the activation and diffusion resistance. The alloy with Fe and Ti:Zr at the atomic ratio 2:1 prepared by using vanadium–ferro-alloy is shown to meet the requirements for the negative electrode in secondary nickel–metal hydride batteries.

1. Introduction

The hydride forming Zr–Ti–V–Ni multicomponent alloys have been tested and adopted for use as negative electrodes in alkaline secondary nickel–metal hydride (Ni–MH) batteries by various research groups [1–10]. Studies on the performance of alloy electrodes have focused on the storage capacity upon charge–discharge cycling, while the kinetics of hydride formation have received little attention [7]. The present work deals with the influence of the alloy composition on their electrochemical behaviour under equilibrium and dynamic conditions. Particular attention has been given to the performance of the alloy containing Fe, prepared by using ferro-alloy as the vanadium source.

2. Experimental details

A series of hydrogen storage alloys of various compositions was prepared by arc-melting under argon atmosphere of appropriate amounts of Zr, Ti, Ni, Cr and V (99.9% Merck), or a much cheaper vanadium–ferro-alloy (80.6%V/18.7% Fe, Baildon). Thereafter, the alloy samples were pulverized (up to 0.03–0.08 mm) in several hydriding–dehydriding cycles. Structure of the electrode material was controlled by XRD measurements using Cu $K\alpha$ radiation.

The electrochemical behaviour of the alloy samples was tested in a three-compartment glass cell with 6 M KOH solution, using a much larger NiOOH/$Ni(OH)_2$ counter electrode and a Hg/HgO/6 M KOH reference electrode. The working electrode was prepared from each pulverized alloy by hot-pressing (under 8000 kg cm^{-2}) to pellet form between nickel nets acting as current-collector. Etching of the electrodes in hot KOH solution for 1 or 2 h, according to the procedure proposed by Reichman *et al.* [3] and Zoitos [11], was sufficient for the initial activation. The specific surface area of the electrode materials determined using the BET technique (ASAP 2010 M, Micromerilitic) was of the order of 1 m^2 g^{-1}. After the first charge–discharge cycle, each alloy electrode exhibited a well activated state and thereafter the discharge capacity remained almost constant.

All electrochemical measurements were carried out in deaerated 6 M KOH solution prepared from Analar grade KOH (POCh Gliwice) and 18 MΩ cm^{-1} water, at 293 K.

Potentiodynamic and galvanostatic techniques with either short or long-term pulses using a conventional apparatus were applied to study the charge–discharge kinetics of the electrodes. The apparatus consisted of a potentiostat (20A Elpan), a wave generator (EG 20 Elpan), a self made galvanostat and an *X-Y* recorder (Riken Denishi). The charge transfer (R_a) and mass transfer resistance (R_d) were estimated from the overpotential against time transients recorded during galvanostatic pulses, at the same depth of charge and/or discharge of different alloy electrodes as proposed by Notten *et al.* [12], after a rest period for potential equilibration. In the measurements of the

* Author to whom correspondence should be addressed.

0021-891X

potentiodynamic j against E (current density against potential) relationships, the potential of the working electrode was swept at a rate of 0.01 to 100 mV s^{-1}. Upon continuous charge–discharge cycling, the alloy electrodes were charged at constant current density (j) to the potential of hydrogen evolution and discharged (at the same current density) down to a cut-off potential of −0.75 V vs Hg/HgO/6 M KOH. In the measurements of the electrochemical pressure–composition (e.p.c.) isotherm, after 10 continuous charge–discharge cycles, the electrode was intermittently charged and discharged under galvanostatic conditions with the resting periods (0.5 h) on open circuit long enough for the potential to equilibriate. The capacity obtained during the discharge was used to calculate the amount of hydrogen absorbed on one mole of the electrode material. Capacity retention studies were conducted after the 20th charge–discharge cycle, whereas a fully charged electrode was left on open circuit for 30 days at 293 K and then discharged again up to the potential $E = -0.75$ V. Hydrogen pressure–composition isotherms (p.c.) for hydrogen absorption–desorption from the gas phase were obtained with a Sievert type apparatus [13].

A sealed button cell of the type Ni–MH KBL 156/066 with alloy $Zr_{10}Ti_{19.2}V_{24.8}Ni_{33.4}Cr_{7.7}Fe_{4.9}$ and $Ni(OH)_2$/NiOOH electrodes in 6 M KOH was constructed and tested in continuous charge–discharge cycles.

3. Results and discussion

Representative alloys investigated in this work are listed in Table 1. In alloys I and II the source of vanadium was the vanadium–ferro-alloy, while the next two alloys III and IV were prepared by using pure metals, as reported by other authors [8–10]. The atomic Ti/Zr ratio was 2:1 for alloy I and III and 1:1 for alloy II and IV; nickel was partly substituted with Fe in alloys I and II. Results of X-ray diffraction analysis enabled us to identify a hexagonal Laves-phase structure in all samples, which is in accordance with the earlier data [5]. The unit cell volumes calculated from the lattice constants for the freshly prepared alloy samples are given in Table 1, along with the data obtained for the alloy samples hydrogenated from the gas phase. The dimensional expansion of a crystal lattice accompanying the hydrogen absorption, due to insertion of H atoms into the interstitial positions, was manifested by a typical shift of the peaks in X-ray diffraction diagrams to lower angles. As expected, this effect was lower for alloys II and IV with a larger unit cell volume in comparison with that of alloys I and III.

Table 1. Unit cell volumes of investigated multicomponent Zr–Ti–V–Ni–Cr–Fe alloys as prepared (V) and after hydrogenation from gas phase (V_h) until p = 0.5 MPa

No.	*Alloy composition* /at %	*Unit cell volume,* $V/(nm)^3$	*Unit cell volume,* $V_h/(nm)^3$
I	$Zr_{10}Ti_{19.2}V_{24.8}Ni_{33.4}Cr_{7.7}Fe_{4.9}$	0.1675	0.1810
II	$Zr_{14.6}Ti_{14.6}V_{24.8}Ni_{33.4}Cr_{7.7}Fe_{4.9}$	0.1715	0.1775
III	$Zr_{10}Ti_{19.2}V_{24.8}Ni_{38.3}Cr_{7.7}$	0.1676	0.1870
IV	$Zr_{14.6}Ti_{14.6}V_{24.8}Ni_{38.3}Cr_{7.7}$	0.1693	0.1742

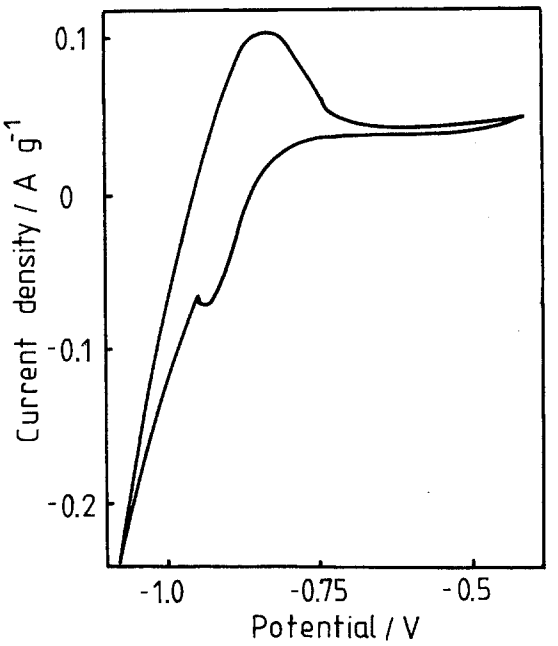

Fig. 1. Cyclic voltammogram of $Zr_{10}Ti_{19.2}V_{24.8}Ni_{33.4}Cr_{7.7}Fe_{4.9}$ alloy electrode in 6 M KOH solution, $v = 0.01$ mV s^{-1}.

3.1. *Electrochemical pressure–composition (EPC) isotherms*

The sorption of hydrogen atoms in the solid phase of the investigated porous alloy electrodes in an alkaline solution is reflected by the hump on the potentiodynamic current density-potential (j against E) curves during the cathodic sweep as illustrated in Fig. 1. It can be seen that this process occurs in the potential range −0.75 to −0.95 V vs Hg/HgO/6 M KOH, prior to hydrogen evolution. The anodic peak appearing on the positive-going sweep is attributed to the oxidative desorption of hydrogen. As exemplified in Fig.2, an increase of hydrogen content in the alloy upon charging of the electrode under galvanostatic conditions is reflected by a sloping potential (E) plateau until the potential of hydrogen gas evolution is reached. The potential is shifted again, almost symmetrically in the positive direction, at the removal and oxidation of the absorbed hydrogen atoms upon discharge. Similar results are also found with the other electrodes.

The electrochemical pressure–composition (e.p.c.) isotherms for absorption and desorption of hydrogen were obtained from the equilibrium potential (E_r) values of the alloy electrodes, measured during an intermittent charge and/or discharge cycles at constant current density, by using the Nernst equation according to the procedure reported by Balej [14]. Figure 2 shows typical equilibrium potential–charge (E_r/Q) curves obtained in the 11th intermittent charge–discharge cycle, after 10 continuous cycles

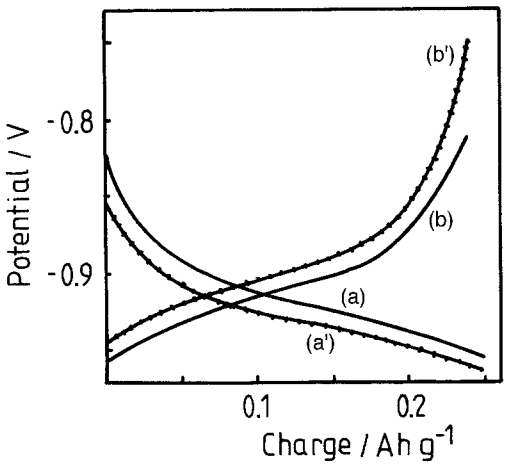

Fig. 2. The equilibrium potential (curves (a) and (b)) and the potential at $j = 40\,\mathrm{mA\,g^{-1}}$ (curves (a′) and (b′)) of $Zr_{10}Ti_{19.2}V_{24.8}Ni_{33.4}Cr_{7.7}Fe_{4.9}$ alloy electrode against charge upon an intermittent charging (curves (a) and (a′)) and discharging (curves (b) and (b′)), after 10 continuous charge–discharge cycles.

for alloy I. It is noticed that the difference in values E_r and E at a given Q is greater for electrodes II and IV than for I and III. The e.p.c. isotherms determined on the alloy electrodes I and II are illustrated in Fig. 3. For the sake of comparison, Fig. 4 shows the storage capacity of these alloys for the hydrogen sorption from the gas phase, as characterized by equilibrium hydrogen pressure against hydrogen content isotherms (p.c.) measured using Sievert equipment. It can be clearly seen that the storage capacity of alloy I (with the Ti:Zr atomic ratio 2:1), working as the negative electrode in a Ni–MH cell, is similar to that at the hydrogen absorption from the gas phase. However, while the electrochemical capacity of alloy

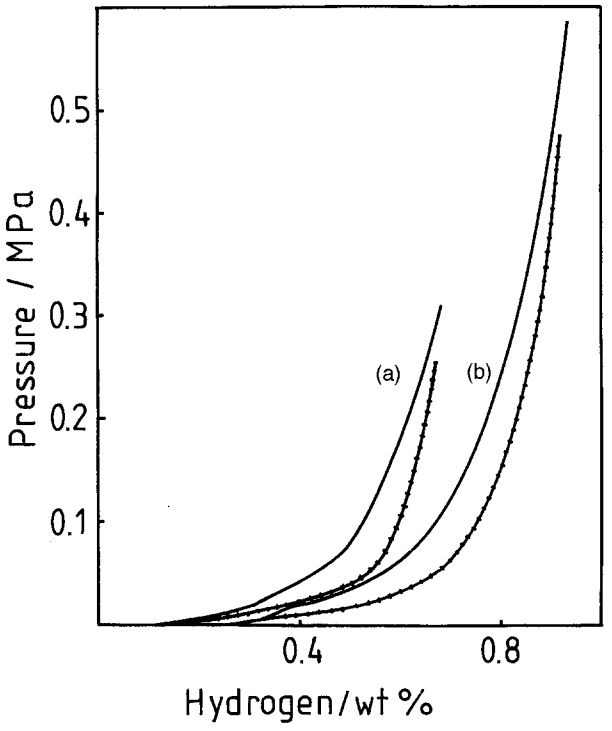

Fig. 3. Electrochemical pressure–composition isotherm for absorption (solid line) and desorption (dotted line) of hydrogen on (a) $Zr_{14.6}Ti_{14.6,}V_{24.8}Ni_{33.4}Cr_{7.7}Fe_{4.9}$ and (b) $Zr_{10}Ti_{19.2}V_{24.8}Ni_{33.4}Cr_{7.7}Fe_{4.9}$, 293 K.

II with increased Zr content (Ti:Zr atomic ratio 1:1) becomes smaller, the amount of hydrogen absorbed from the gas phase increases. Analogous regularities are obtained for alloys III and IV. Again, the electrochemical capacity of alloy electrode IV, with an increased Zr content, is smaller than that of alloy III, while a reversed dependence is observed for hydrogen absorbed from the gas phase. These results point to differences in the surface state of alloy particles in the electrode material in an alkaline solution and in the hydrogen gas atmosphere. The electrochemical oxidation of the particle surface in an alkaline solution, along with formation of a passive layer, which inhibits the hydrogen electrosorption into the electrode material, are favoured on alloy samples (II and IV) containing more Zr. A larger amount of the electrochemically absorbed hydrogen found for alloys I and III with an increased Ti:Zr ratio can be explained by an easier dissolution of the surface oxide upon charge–discharge cycling. Furthermore, it should be noted that De Pauli *et al.* [15] have observed loading of the TiO_2 films with hydrogen to occur in acidic solution. The same might be expected in an alkaline solution.

As follows from the E_r/Q and E/Q curves as well as from the e.p.c. isotherms for alloys with Ti:Zr atomic ratio 2:1, the hydrogen storage capacities of alloy I with a part of Ni substituted by Fe and of alloy III without Fe are quite similar. The E_r/Q curves of alloy I with Fe are only slightly shifted towards more negative potentials relative to the corresponding curves for alloy III without Fe. Accordingly, the values of the equilibrium hydrogen pressure on electrode I are slightly higher at the same charge and/or discharge level. However, both these alloys reveal comparable coulombic charge/discharge efficiency, which will be discussed below.

3.2. *Influence of alloy composition on the kinetics of the electrochemical hydrogen sorption-desorption*

The kinetics of the absorption–desorption of hydrogen on the investigated, uncycled and cycled, alloy electrodes was estimated under potentiodynamic and galvanostatic conditions.

Figure 5 shows typical current density against potential relationships recorded in the vicinity of the equilibrium potential for the chemically activated, as well as for the charged and discharged, alloy electrodes I. The j against E plot for the electrode in an activated and/or charged state is linear with almost the same slope for the anodic and cathodic branches, thus proving the reversibility of hydrogen electrosorption–desorption. Because of the absence of any effect of the sweep rate on the current values, the slope can be treated as a measure of the charge transfer resistance ($R_{a(p)} = \mathrm{d}E/\mathrm{d}j$). It ranges from 0.31 to $1.3\,\Omega\,\mathrm{g}^{-1}$ (Table 2). A lower R_a value for alloy I and III and correspondingly higher exchange current density (calculated from R_a by the equation: $j_o = RT/FT_a$) provides evidence for improved

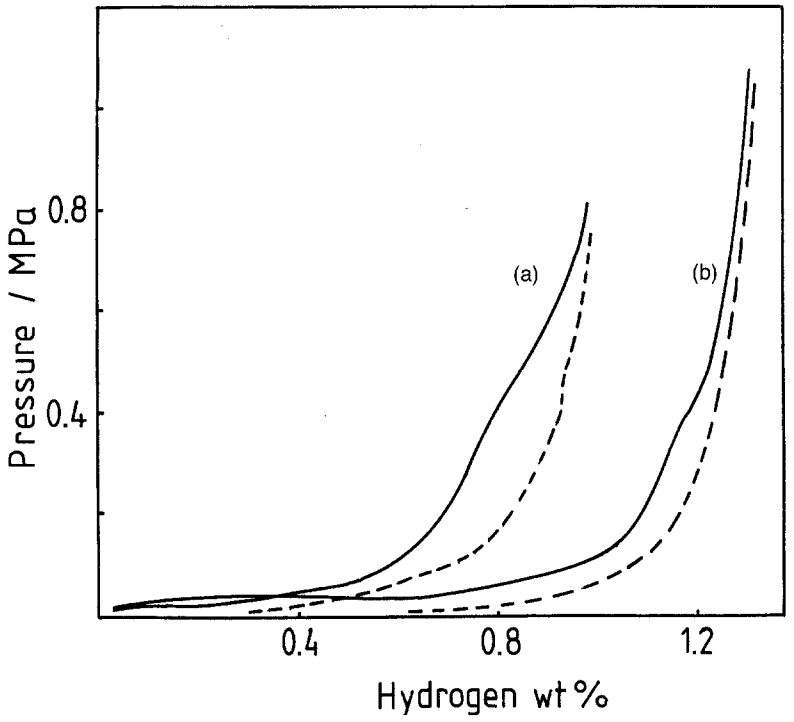

Fig. 4. Pressure–composition isotherm for absorption (solid line) and desorption (dashed line) of hydrogen from the gas phase at 293 K on (a) $Zr_{14.6}Ti_{14.6}V_{24.8}Ni_{33.4}Cr_{7.7}Fe_{4.9}$ and (b) $Zr_{10}Ti_{19.2}V_{24.8}Ni_{33.4}Cr_{7.7}Fe_{4.9}$.

catalytic activity of the alloys in the hydrogen electrosorption-desorption reaction in comparison with that of alloy II and IV.

As can be seen from Fig. 5, the charge transfer resistance is strongly affected by the state of the electrode material. The j against E plots are shifted to more positive potentials and R_a increases with depth of discharge, whereas it is smaller again for alloy I and III in comparison with alloy II and IV. Similar dependencies also result from the galvanostatic single-pulse measurements of the E against t transients, which provides a distinction between the charge transfer and diffusion resistance. Figure 6 illustrates the overpotential against time (η against t) curves recorded during anodic and cathodic galvanostatic pulses at $j = 40\,\mathrm{mA\,g^{-1}}$ on the fully charged and fully discharged electrode I. It should be noted that the anodic and cathodic parts of these curves, for the charged electrode as well as for the discharged ones, are symmetrical with respect to the time axis. This means that the value of the overpotential measured after an arbitrary lapse of time after the start of the galvanostatic pulse is independent of the direction of the current. In this way the reversibility of the electrode processes is confirmed. Analysis of the η against t data obtained for the first 15 s points to a linear dependence of the overpotential with the square root of time, predictable for time variations of the diffusion overvoltage at $j = \mathrm{const}$ [16]. The $\mathrm{d}E/j\ \mathrm{d}t^{1/2}$ value, considered as a measure of the changes in diffusion resistance (R_d), ranges from 0.01 to $0.05\,\Omega\,\mathrm{s}^{1/2}$ for the investigated electrodes in an activated and charged state. Thus, the diffusion of hydrogen in the solid phase of alloy electrodes appears to be rapid. A high rate of the hydrogen diffusion in the solid phase of alloy electrodes is also indicated by a fast potential equilibration after interruption of the circuit. It is

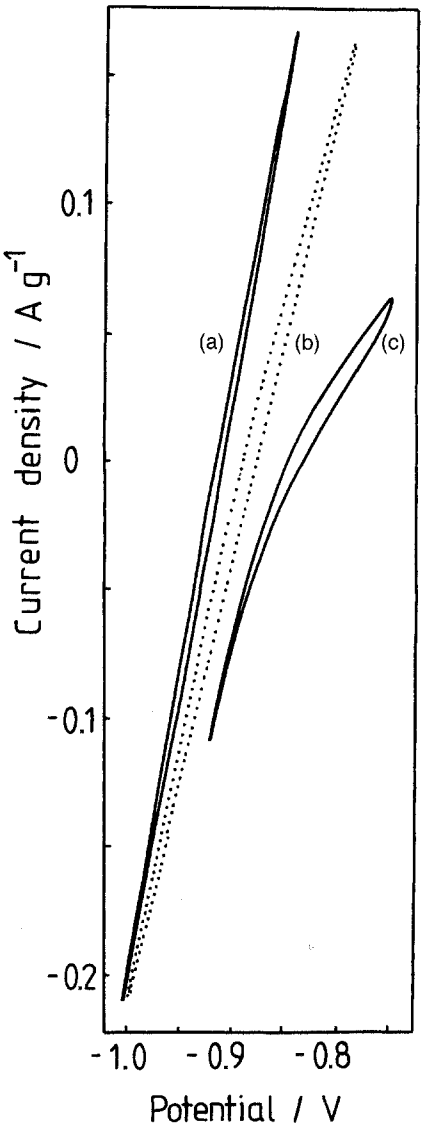

Fig. 5. Current density against potential for $Zr_{10}Ti_{19.2}V_{24.8}Ni_{33.4}Cr_{7.7}Fe_{4.9}$ alloy electrode in 6 M KOH (a) in the charged state, (b) after chemical activation and (c) after discharge, $v = 10\,\mathrm{mV\,s^{-1}}$.

Table 2. Charge transfer resistance from galvanostatic measurements $R_{a(g)}$ and from potentiodynamic measurements $R_{a(p)}$ for hydrogenated from the gas phase, chemically activated Zr–Ti–V–Ni–Cr–Fe alloy electrodes (1, 1′, after 1 h activation; 3, after 2 h activation) and for electrochemically hydrogenated, fully charged electrodes (2, 2′)

No.	*Alloy composition*	*1*	*1′*	*2*	*2′*	*3*
		$R_{a(g)}$ /Ω g^{-1}	$R_{a(p)}$ /Ω g^{-1}	$R_{a(g)}$ /Ω g^{-1}	$R_{a(p)}$ /Ω g^{-1}	$R_{a(g)}$ /Ω g^{-1}
I	$Zr_{10}Ti_{19.2}V_{24.8}Ni_{33.4}Cr_{7.7}Fe_{4.9}$	0.43	0.55	0.37	0.45	0.35
II	$Zr_{14.6}Ti_{14.6}V_{24.8}Ni_{33.4}Cr_{7.7}Fe_{4.9}$	1.3	1.5	0.75	0.83	1.2
III	$Zr_{10}Ti_{19.2}V_{24.8}Ni_{38.3}Cr_{7.7}$	0.34	0.45	0.31	0.38	0.25
IV	$Zr_{14.6}Ti_{14.6}V_{24.8}Ni_{38.3}Cr_{7.7}$	0.54	0.65	0.49	0.53	0.44

typical of the reversible hydrogen electrosorption–desorption at the surface of alloy samples, that the values of the overpotential estimated after extrapolation of the E against $t^{1/2}$ relationship to $t = 0$ are independent of the direction of the current. The charge transfer resistance values obtained from the galvanostatic $\eta_{t=0}$ against j plot ($R_a = d\eta_{t=0}/dj$) for 1 h in a hot KOH solution activated electrodes as well as for fully charged alloy electrodes (Table 2) are, within the limits of experimental error, in accordance with those values obtained for the same electrodes from the potentiodynamic measurements.

The increase in the charge transfer and diffusion resistance at the end of discharge of an electrode material can be clearly seen in Fig. 6. For the discharged electrodes, the activation resistance (R_a) values are about twice and the diffusion resistance (R_d) about ten times greater than the corresponding values for the charged electrodes. This effect must be connected with the overlap of the oxidation of absorbed hydrogen and of the formation/dissolution of passive oxides on the alloy particle surface.

No significant differences are found in the kinetic parameters of hydrogen absorption–desorption on the alloy electrodes I and III containing Fe from the vanadium–ferro-alloy and without Fe, respectively.

Figure 7 presents the E against t transients recorded in the experiments performed to study the behaviour of the chemically activated alloy electrode I at various charge and discharge rates prior to the continuous charge–discharge cycling. The time of chemical activation of the electrode material was in this case prolonged to 2 h. It can be seen that the anodic and cathodic parts of the E against t curves are almost symmetrical with respect to the time axis, even at the rate of charge and /or discharge of 1/2 C. Similar results are obtained for electrode III. It may be concluded that for these materials fast discharge rates can be achieved. The diffusion of hydrogen in the solid phase of these alloy electrodes determines the overall charge–discharge rate only at a deep depth of discharge (Fig. 6). In the case of alloy II, on the other hand, at relatively low current densities, a high diffusion resistance is found to occur in the hydrogen electrosorption–desorption process. Kinetic parameters for electrode IV fall in-between those obtained for electrodes I and II. These results indicate that the rate determining step varies, depending on the composition of hydrogen storage alloy, the discharge rate and the discharge depth.

It is worth noting that extension of the activation of alloys in a hot KOH solution to 2 h brings about a decrease of R_a relative to the corresponding values for the 1 h activated electrodes (Table 2). This can be linked to a larger specific surface of the electrode, as well as to an increased porosity of the oxide film

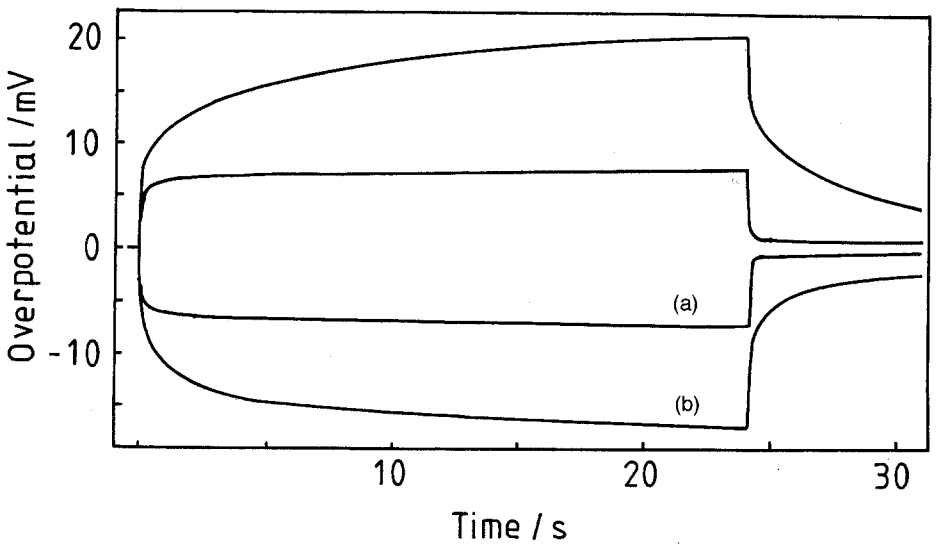

Fig. 6. Overpotential against time during anodic and cathodic galvanostatic pulses, $j = 40\,mA\,g^{-1}$, on (a) charged ($E_r = -937\,mV$) and (b) discharged ($E_r = -838\,mV$) $Zr_{10}Ti_{19.2}V_{24.8}Ni_{33.4}Cr_{7.7}Fe_{4.9}$ electrode, in the 10th continuous charge–discharge cycle.

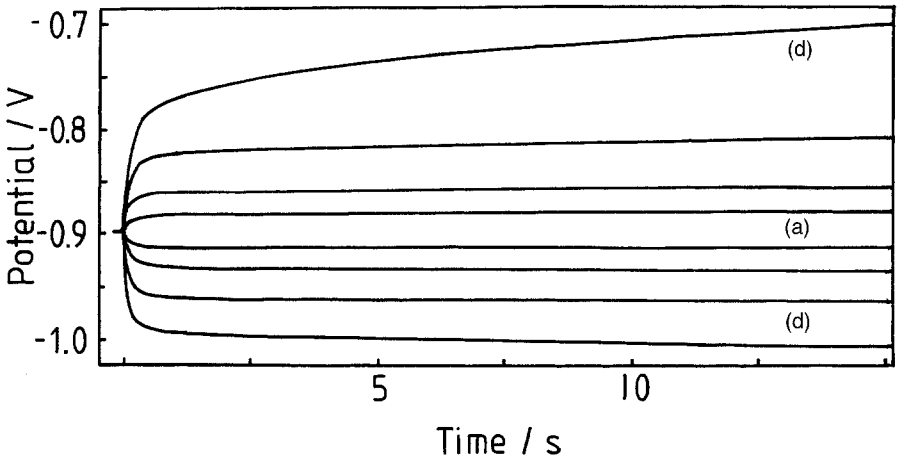

Fig. 7. Potential against time at various current densities on chemically activated $Zr_{10}Ti_{19.2}V_{24.8}Ni_{33.4}Cr_{7.7}Fe_{4.9}$ electrode during anodic and cathodic galvanostatic pulses (a) 40, (b) 80, (c) 160 and (d) 320 mA g^{-1}.

at the interface between the solid phase and the electrolyte solution. This problem, however, requires further investigation.

The enhanced rate of electrosorption of hydrogen atoms and diffusion for alloys with Ti:Zr at the atomic ratio 2:1, evidenced by smaller R_a and R_d values, may be explained in terms of the synergistic effect invoked by interaction between Zr, Ti, V and Ni or Fe, as well as by a higher resistance of the alloy surface towards passivation with an increase in titanium content. Here, the effect of the lower lattice volume of the I and III alloys on the hydride stability must be of secondary importance.

3.3. *Alloy performance in Ni–MH batteries*

According to the kinetic data and the e.p.c. isotherms, good rechargeability was expected, in particular, for alloy electrodes I and III. This was confirmed by the long-term charge–discharge continuous cycling experiments. As shown by the typical potential against charge (E/Q) curves in Fig. 8, alloy electrodes I and III, display a comparable high hydrogen storage capacity and coulombic efficiency of the hydrogen electrosorption–desorption reaction. The amount of charge yielded upon the discharge of alloy I and III to $E = -0.75$ V was always of about $94 \pm 2\%$ of the charge supplied to the electrode in the appropriate potential range and at the appropriate current density. The discharge capacity value of 0.240 Ah g^{-1} is in a good agreement with the data reported by Fetcenko *et al.* [4] for the AB_2-type alloys. It seems reasonable to conclude that these considerable capacities, maintained at the same level during the repeated charge–discharge cycles, are caused by a high diffusion rate of hydrogen atoms in the solid phase of the alloy electrodes. A relatively slight difference is observed only for the potential values of both alloys at the same charge or discharge depth. The values of the potential of alloy I, with Ni partly substituted by Fe, are more negative in comparison with the corresponding values for alloy III, without Fe, as in the case of the intermittent charge–discharge cycles. The charge/discharge capacity decreases with decreasing Ti:Zr ratio. The lower coulombic discharge efficiency of $85 \pm 2\%$ and $87 \pm 2\%$ was achieved by continuously cycling alloy electrodes II and IV, characterized by both an increased activation and diffusion resistance. The last alloy electrodes yielded a discharge capacity of about 0.180 Ah g^{-1} and 0.210 Ah g^{-1}, respectively.

3.4. *Self discharge*

Typical discharge curves (E/Q) measured on the fully charged electrodes I after 30 days of storage at open

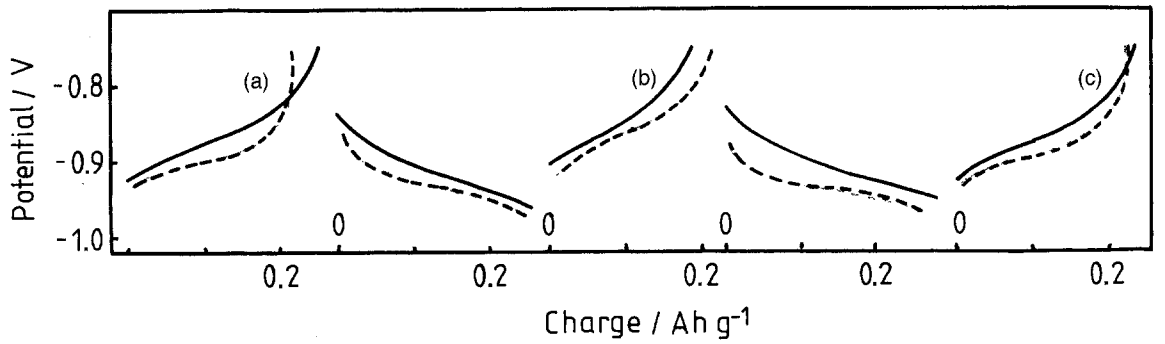

Fig. 8. Potential of $Zr_{10}Ti_{19.2}V_{24.8}Ni_{33.4}Cr_{7.7}Fe_{4.9}$ electrode (dotted line) and of $Zr_{10}Ti_{19.2}V_{24.8}Ni_{38.3}Cr_{7.7}$ electrode (solid line) against charge during cycling at (a) discharge in the 20th cycle, (b) discharge after 30 day storage at open circuit after charging to a depth of 100%, (c) discharge in the 22th cycle, $j = 40$ mA g^{-1}.

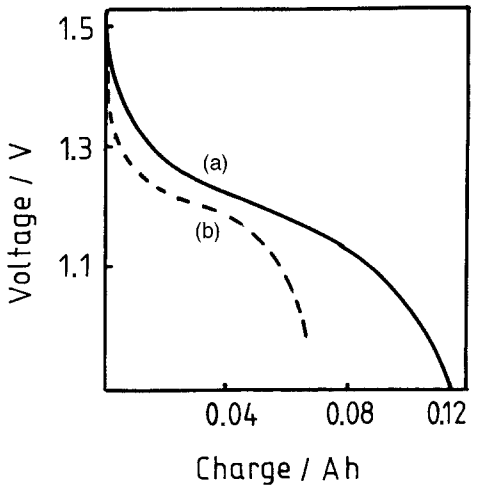

Fig. 9. Discharge curve of a button sealed cell KBL 156/066 (a) of type Ni–MH with $Zr_{10}Ti_{19.2}V_{24.8}Ni_{33.4}Cr_{7.7}Fe_{4.9}$ at $I = 20\,mA$, after charging to a depth of 100% at $I = 10\,mA$ and (b) of type Ni–Cd at $I = 20\,mA$, after charging to a depth of 100% at $I = 6\,mA$.

circuit at 293 K are included in Fig. 8. By comparing the discharge capacity restored in the investigated samples with that obtained during the proceeding and in the next continuous charge–discharge cycle, it may seen that the self discharge rate was relatively small. The capacity loss in the conditions of the open circuit was of about 20%, similar to that proper for Ni–Cd battery. Here again, alloys I and III have some advantages over alloys II and IV, which show a higher self discharge rate.

3.5. *Alloy performance in sealed button cells*

As indicated above, the electrochemical properties of alloy I and of alloy III are very similar, with the first alloy (prepared using ferro-alloy as a source of vanadium) being markedly cheaper. Therefore, alloy I was chosen as a negative electrode material for the sealed button cell of type Ni–MH KBL 156/066 constructed in our laboratory using the same $NiOOH/Ni(OH)_2$ electrode as in the sealed Ni–Cd battery. As shown in Fig. 9, the storage capacity of the Ni–MH battery with alloy I as the negative electrode is clearly higher than that of the Ni–Cd battery.

4. Conclusions

It may be concluded that the electrochemical properties of the Zr–Ti–V–Ni–Cr–Fe and Zr–Ti–V–Ni–Cr alloy materials improve with increasing Ti:Zr ratio. Both the rate of hydrogen electrosorption–desorption as well as the amount of absorbed hydrogen atoms were found to be higher for alloys with the Ti:Zr at atomic ratio 2:1 in comparison with that for the alloys containing Ti and Zr at the ratio 1:1. The economically interesting alloy of composition $Zr_{10}Ti_{19.2}V_{24.8}Ni_{33.4}Cr_{7.7}Fe_{4.9}$ in an alkaline solution displays an excellent reversibility for the electrochemical hydrogen absorption–desorption reaction.

Acknowledgements

This work was financially supported by Komitet Badań Naukowych, Poland, within research project 8.5502 083 04. The authors also thank Prof. dr hab. H. Drulis of the Institute of Low Temperature and Structure Research, Polish Academy of Sciences, Wrocław for supplying the alloy samples characterized by gas-phase isotherms.

References

[1] M. A. Fetcenko, S. Vanketasan and S. R. Ovhinsky, Proceedings of the symp. on 'Hydrogen Storage Materials, Batteries and Electrochemistry' (edited by A. Dennis), Pennigton NY, **5** (1992) 141.
[2] M. A. Fetcenko, S. Vanketasan, K. C. Hong and B. Reichman, 16th International Power Sources Symposium, Brighton, UK (1988).
[3] B. Reichman, S. Vankatesan, M. A. Fetcenko, K. Jeffries, S. Stahl and J.Bennnett, *US Patent 4 716 088* (1988).
[4] M. A. Fetcenko and S .Vanketasan, *Progr. Batteries* **9** (1990) 259.
[5] H. Miyamura, T. Sakai, N. Kuriyama, K. Oguro, A. Kato and H. Ishikawa, *in* A. Dennis (ed.), *op. cit.* [2] **5** (1992) 179.
[6] S. Wakao, H. Sawa and J. Furukawa, *J. Less Common Metals*, **172–174** (1991) 1219.
[7] C. Iwakura and M. Matsuoka, *Progr. Batteries* **10** (1991) 81.
[8] M. A. Fetcenko and R. Oak, *US Patent 5 096 667* (1992).
[9] J. Y. Lee and J. M. Park, *US Patent 5 028 389* (1991).
[10] K. Sapru, K. Hong , M. A. Fetcenko and S.Vanketasan, *US Patent 4 551 400* (1985).
[11] B. K. Zoitos, D. L. Hudson, P. D. Bennett and V. J. Puglisi, *in* A. Dennis (ed.), *op. cit.* [2] **5** (1992) 168.
[12] P. Notten and R. Einerhand, *Adv. Mater.* **3** (1991) 343.
[13] A. Sievert and A. Gatta, *Z. Anorg. Chem.* **172** (1928) 1.
[14] J. Baley, *Int. J. Hydrogen Energy* **10** (1985) 363.
[15] R. M. Torresi, O. R. Camara and C. P. De Pauli, *Electrochim. Acta* **32** (1987) 1357.
[16] S. Atlung, K. West and T. Jacobsen, *J. Electrochem. Soc.* **126** (1979) 1311.